

## X-ray emission from the terrestrial magnetosheath including the cusps

I. P. Robertson,<sup>1</sup> M. R. Collier,<sup>2</sup> T. E. Cravens,<sup>1</sup> and M.-C. Fok<sup>2</sup>

Received 15 February 2006; revised 12 May 2006; accepted 24 July 2006; published 14 December 2006.

[1] X rays are produced throughout the terrestrial magnetosheath as a consequence of charge transfer collisions between heavy solar wind ions and exospheric neutrals. The solar wind ions resulting from these collisions are left in highly excited states and emit extreme ultraviolet or soft X-ray photons. We previously simulated X-ray images of the magnetosheath as seen from an observation point outside the geocorona for average solar wind conditions. The locations of the bow shock and magnetopause were evident in these images, but the cusps were not taken into account. For the current paper we used dynamic three-dimensional MHD simulations of the solar wind, magnetosheath, and magnetosphere for the 31 March 2001 geomagnetic storm. A sky map was generated of the expected X-ray emissions as seen by a hypothetical X-ray detector on the IMAGE spacecraft. Modeled images as seen from an observation point well outside the geocorona were also created. The cusps can clearly be detected in both types of simulated images. Images of the magnetosheath in energy neutral atoms (ENA) also show the cusps. X-ray imaging of the magnetosheath, revealing the structure of the magnetopause and the bow shock, if carried out, could potentially make a valuable contribution to our understanding of the solar wind interaction with the magnetosheath.

**Citation:** Robertson, I. P., M. R. Collier, T. E. Cravens, and M.-C. Fok (2006), X-ray emission from the terrestrial magnetosheath including the cusps, *J. Geophys. Res.*, *111*, A12105, doi:10.1029/2006JA011672.

### 1. Introduction

[2] In 1996, X-ray emission from the comet Hyakutake was discovered [Lisse *et al.*, 1996]. Cravens [1997] proposed that this type of X-ray emission could be produced by charge exchange between heavy solar wind ions and cometary neutrals. In the solar wind charge exchange (denoted SWCX from now on) mechanism, an electron is transferred from a neutral target atom or molecule to a high charge state heavy solar wind ion. The electron in the heavy ion is left in an excited state and emits a photon in the extreme ultraviolet (EUV) or soft X-ray regions of the spectrum when the ion makes transitions to lower states. To date, similar X-ray emissions from a large number of comets and planets, interstellar gas throughout the heliosphere, and even the moon (actually from the terrestrial geocoronal hydrogen) have been observed. For a review of cometary and planetary X-ray emission, see review papers by Krasnopolsky *et al.* [2005], Cravens [2002], Lisse *et al.* [2005], and Bhardwaj *et al.* [2002].

[3] X rays and EUV radiation from the SWCX mechanism vary with time, which can be attributed to (1) temporal variations in the solar wind proton flux [Neugebauer *et al.*, 2000; Lisse *et al.*, 1999] and (2) variations in the relative solar wind heavy ion composition [Neugebauer *et al.*, 2000;

Schwadron and Cravens, 2000]. The first source of variability appears to dominate at least at shorter timescales in that the solar wind proton flux has been demonstrated to correlate quite well with X-ray emission at comets [Neugebauer *et al.*, 2000] and at Earth [Cravens *et al.*, 2001; Robertson and Cravens, 2003]. Cravens [2000] constructed a simple model of X-ray emission from charge exchange between heavy solar wind ions and interstellar helium and hydrogen and geocoronal hydrogen and showed that most of the X-ray time variations came from the solar wind interaction with geocoronal hydrogen in the magnetosheath. A more sophisticated model of the magnetosheath X-ray emission [Robertson and Cravens, 2003] used published terrestrial exospheric hydrogen densities [Hodges, 1994] and used solar wind speeds, solar wind densities, and temperature distributions in the magnetosheath from a numerical hydrodynamic model [Spreiter *et al.*, 1966]. Average upstream solar wind conditions were adopted with a density of  $7 \text{ cm}^{-3}$  and a solar wind speed of 400 km/s. For these conditions the subsolar distance to the magnetopause is  $9.5 R_E$ . Robertson and Cravens [2003] suggested that it might be possible to remotely sense the magnetosheath from outside the bow shock using X-ray emission.

[4] Observational evidence of solar wind charge exchange with geocoronal and interstellar neutrals producing X rays was also obtained from the XMM-Newton X-ray telescope. XMM-Newton observations showed several spectral lines characteristic of the SWCX mechanism [Snowden *et al.*, 2004] for lines-of-sight traversing the magnetosheath. And characteristic SWCX spectral lines from only the geocoronal hydrogen (i.e., no heliospheric or “cosmic” contributions) were observed by the Chandra

<sup>1</sup>Department of Physics and Astronomy, University of Kansas, Lawrence, Kansas, USA.

<sup>2</sup>Heliospheric Physics, NASA Goddard Space Flight Center, Greenbelt, Maryland, USA.

X-Ray Observatory (CXO) during observations of the “dark” side of the moon [Wargelin *et al.*, 2004].

[5] The magnetosheath has also been observed using energetic neutral atoms (ENA). Remote observations of the magnetosheath were made by the Low Energy Neutral Atom (LENA) imager on the IMAGE spacecraft [Collier *et al.*, 2001, 2005]. During periods of high solar wind ram pressure, when the magnetopause was close to the Earth, LENA observed “diffuse” ENAs resulting from the post-shock solar wind protons exchanging charge with exospheric hydrogen. Observations have also shown evidence that LENA can observe the cusp in the same way [e.g., Moore *et al.*, 2003; Taguchi *et al.*, 2004; Taguchi *et al.*, 2005].

[6] The solar wind parameters for the current paper are taken from MHD simulations of the 31 March 2001 coronal mass ejection event. This event caused the magnetopause to be pushed in to near geosynchronous orbit at 6.6  $R_E$  [Fok *et al.*, 2004; Collier *et al.*, 2001]. In this paper we will (1) review the SWCX mechanism for the magnetosheath and the cusps, (2) present modeled observations as seen from inside the magnetosheath by a hypothetical X-ray detector on the IMAGE spacecraft, and (3) present modeled observations as seen by an observer far outside the magnetosheath. The cusps are “indentations” of the magnetopause in the polar regions at which solar wind plasma can penetrate close to Earth [Reiff *et al.*, 1977]. We will demonstrate the dramatic time variation of the terrestrial X-ray emission by comparing these new images with images shown in our previous publications. And we will show that because of the time variations, observing the SWCX X-ray emissions might be an additional method (and motivation) for studying the properties of the magnetosheath.

## 2. Charge Exchange Model

### 2.1. Solar Wind Charge Exchange Mechanism

[7] Ions in the solar wind can undergo charge exchange collisions with neutrals. The product ion will invariably be left in an excited state and the excited ion emits a photon [cf. Cravens, 2002]. For highly charged solar wind ions the photons are in the EUV or X-ray part of the spectrum. For example, the charge exchange between a heavy oxygen ion and neutral hydrogen can be represented by



The captured electron in  $O^{6+*}$  is highly excited, and as it cascades down to the ground state it emits a photon in the X-ray region of the spectrum [cf. Kharchenko and Dalgarno, 2000]. For SWCX with interstellar neutrals, the most abundant neutral species are atomic hydrogen and helium. For SWCX near Earth, the most abundant neutral species is exospheric atomic hydrogen. Heavy solar wind ions ( $Z > 2$ ) are only 0.1% of the solar wind but are responsible for the X-ray emissions. In this study we will only consider X-ray emission (the 100 eV to 1 keV energy band) due to SWCX between heavy solar wind ions and geocoronal neutral hydrogen.

[8] To calculate the SWCX X-ray intensity in a particular look direction, we need to first determine the X-ray pro-

duction rate, or volume emission rate, at each point along the line of sight. This production rate is given by

$$P_{X-ray} = \alpha n_H n_{sw} \langle g \rangle (eV \text{ cm}^{-3} \text{ s}^{-1}) \quad (2)$$

where  $\alpha$  is a soft X-ray emission efficiency factor which is dependent upon the relative abundance of heavy ions in the solar wind and the average charge transfer cross section for high charge state heavy ions, integrated over photon energy [cf. Schwadron and Cravens, 2000]. Here  $n_H$  is the neutral terrestrial exospheric hydrogen number density,  $n_{sw}$  is the local solar wind density, and  $\langle g \rangle$  is the average total ion speed, which can be expressed in terms of both bulk and thermal speeds.

[9] The X-ray efficiency factor  $\alpha$  depends on solar wind composition, which in turn depends on whether the solar wind is fast or slow [Schwadron and Cravens, 2000; Kharchenko and Dalgarno, 2000]. For a slow solar wind (with a velocity between 300 and 600 km/s) Pepino *et al.* [2004] determined that  $\alpha = 9.38 \times 10^{-16} \text{ eV cm}^2$ . Similarly, for a fast solar wind (with a velocity between 600 and 800 km/s)  $\alpha = 3.33 \times 10^{-16} \text{ eV cm}^2$ . For a coronal mass ejection this efficiency factor could be even less. For convenience, the efficiency factor used for the current paper is  $6 \times 10^{-16} \text{ eV cm}^2$ , which is identical to the efficiency factor used by Robertson and Cravens [2003] in their previous paper on solar wind charge exchange with geocoronal hydrogen. The X-ray intensity in a given direction is determined by integrating the production rate along the line of sight.

### 2.2. Average Solar Wind Parameters

[10] Near Earth, the average unperturbed solar wind density is  $7 \text{ cm}^{-3}$ . After the supersonic solar wind passes the bow shock and enters the magnetosheath, the solar wind slows down, heats up and flows around the magnetosphere. The solar wind reaches its highest density in the subsolar region of the magnetosheath, with an increase of as much as a factor of 4 [Spreiter *et al.*, 1966]. The solar wind temperature is also at its highest values in the subsolar region; the unperturbed solar wind temperature can increase by as much as a factor of about 20. Since most of the solar wind does not penetrate inside the magnetopause, its bulk speed,  $u$ , is at a minimum near the subsolar point.

[11] Normally, the average collision speed  $\langle g \rangle$  is very close to the solar wind speed  $u$  in the unshocked solar wind. In the magnetosheath region much (or most) of the bulk kinetic energy of the solar wind flow has been converted to thermal energy, and the thermal speed  $v_{\text{thermal}}$  becomes an important contributor to  $\langle g \rangle$ . The thermal speed is calculated as follows:

$$v_{\text{thermal}} = \sqrt{\frac{3k_B T}{m}} \quad (3)$$

where  $m$  is the mass of a solar wind proton and  $T$  is the temperature of the solar wind at the location in question. The assumption is made that the kinetic temperature ratio of the heavy solar wind ion scales with its mass (i.e., that thermal velocities for different ion species are the same) in agreement with observation [cf. Ogilvie *et al.*, 1980;

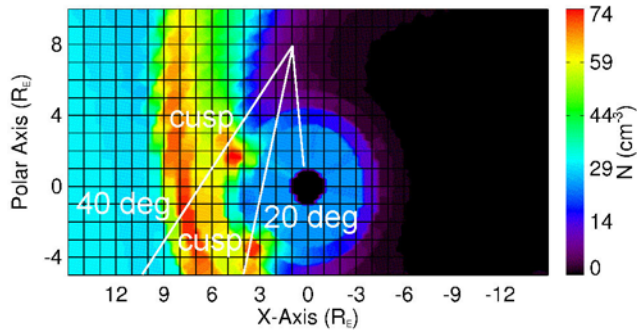


**Figure 1.** Orbital plane of IMAGE spacecraft, which coincides with the GSM x-z plane. Plasma densities from an MHD simulation are shown with values indicated by the color bar. Distance units are Earth radii. The 20° and 40° spin angle lines of sight from IMAGE intersect the cusps. The x axis is along the Earth-Sun line. The time of simulation is 31 March 2001, 0440 UT.

*Bochsler et al.*, 1985; *Collier et al.*, 1996; *Feynman*, 1975]. We realize, however, that significant deviations from this relationship are frequently observed [cf. *Ogilvie et al.*, 1980; *Bochsler et al.*, 1985; *Collier et al.*, 1996; *Feynman*, 1975]. The root mean square solar wind speed is given by

$$\langle g \rangle = \sqrt{u^2 + v_{\text{thermal}}^2} \quad (4)$$

### 2.3. Geocoronal Neutral Hydrogen

[12] Solar wind ions can charge exchange with geocoronal neutral hydrogen in the magnetosheath and in the cusp regions. The neutral hydrogen density varies spatially, with a primary maximum in the antisolar direction, and a secondary maximum in the solar direction. Previously, *Robertson and Cravens* [2003] adopted neutral hydrogen densities from the *Hodges* [1994] Monte Carlo model. In a simpler version of the X-ray model, *Cravens et al.* [2001] used an expression  $n_H = n_{H0}(10 R_E/r)^3$  with  $n_{H0} = 25 \text{ cm}^{-3}$  to approximate the *Hodges* [1994] density profiles in the vicinity of the magnetopause (near  $10 R_E$ ). We have also used this approximation in the current paper.

### 2.4. CCMC and the 31 March 2001 Coronal Mass Ejection

[13] On 31 March 2001 a massive coronal mass ejection struck the Earth, creating the largest geomagnetic storm of that solar cycle. Distance to the subsolar point of the magnetopause depends on solar wind density and solar wind speed [*Chapman and Ferraro*, 1931]. For average solar wind conditions ( $n_{\text{sw}} \sim 7 \text{ cm}^{-3}$ ,  $v_{\text{sw}} \sim 400 \text{ km/s}$ ) the distance to the subsolar region of the magnetopause is around  $9.5 R_E$ ; however, during the 31 March 2001 storm the solar wind speed and density increased so much that the magnetopause was pushed inside the geostationary orbit at  $6.6 R_E$  [*Baker et al.*, 2002]. Since for a short period the interplanetary magnetic field was also southward, the solar wind was able to enter the magnetosphere relatively easily.

[14] At the Community Coordinated Modeling Center (CCMC) at Goddard Space Flight Center, the BATSRUS MHD model was used to create three-dimensional simulations of Earth’s magnetosheath and magnetosphere during this 31 March 2001 event [*Fok et al.*, 2004]. This model was originally developed at the University of Michigan [*Groth et al.*, 2000]. The resulting simulation data contained plasma temperatures, velocities, and densities on a nonuniform grid in a region of about  $50 R_E$  surrounding Earth. Our first task was to distinguish in this MHD output the solar wind plasma from magnetospheric plasma. The plasma density near the subsolar region of the magnetopause (where the solar wind density peaks) was used to locate the boundary for this storm event. We found this to be at around  $6 R_E$ . *Spreiter et al.* [1966] generated maps in which they displayed contour lines for solar wind speed, temperature and density within the magnetosphere. We found an expression, using the *Spreiter et al.* [1966] contour maps for the magnetopause location in terms of D (distance to the subsolar magnetopause). This equation was used to locate the magnetopause boundary in the MHD data file. In the cusp regions, however, solar wind plasma can extend all the way to the Earth [*Reiff et al.*, 1977]. Since we can expect a higher solar wind density in the cusps, we defined them to be regions within the “nominal Spreiter magnetosphere,” where the density was higher than  $40 \text{ cm}^{-3}$ . Figure 1 shows a density plot in the GSM x-z plane generated by the BATSRUS model. The cusps can clearly be seen. In Figure 1 the IMAGE spacecraft orbit is projected on to the GSM x-z plane, which is approximately the orbital (x-y) plane of the spacecraft at that time.

[15] We determined what spatial points along a line of sight are outside the magnetosphere or in the cusps, and then all production rates are calculated. The nearest neighbor method is used to determine the solar wind density, velocity and temperature at any point along a line of sight using the gridded raw neutral data. The total intensity is calculated by integrating X-ray production rates along the line of sight.

[16] *Robertson and Cravens* [2003] used a line of sight of  $100 R_E$ , whereas we only have information for a region that extends outwards from Earth for about  $50 R_E$ . However,  $50 R_E$  is well beyond the bowshock, particularly in the upwind direction, and the hydrogen density tapers off as  $1/r^3$ . Hence the contribution of the region beyond  $50 R_E$  to the X-ray intensity is negligible.

[17] The SM coordinates (x, y, z) of the IMAGE spacecraft at the time of observation were [1.972,  $-0.14$ , 7.8] in units of  $R_E$ . The SM x-z plane coincides closely with the GSM x-y plane. IMAGE is a spinning spacecraft; the z axis is along the spin axis of the spacecraft and the spin angle is defined as zero when the instrument points toward the Earth. The spin axis (z) is approximately perpendicular to the orbit plane. In Figure 1 a few lines of sight are plotted. A line of sight with a spin angle of about 20 degrees intersects the lower cusp but does not intersect the high-density subsolar region. On the other hand, a line of sight with a spin angle of 40 degrees will intersect the upper cusp and also the lower section of the subsolar region. Both cusps therefore should be discern-

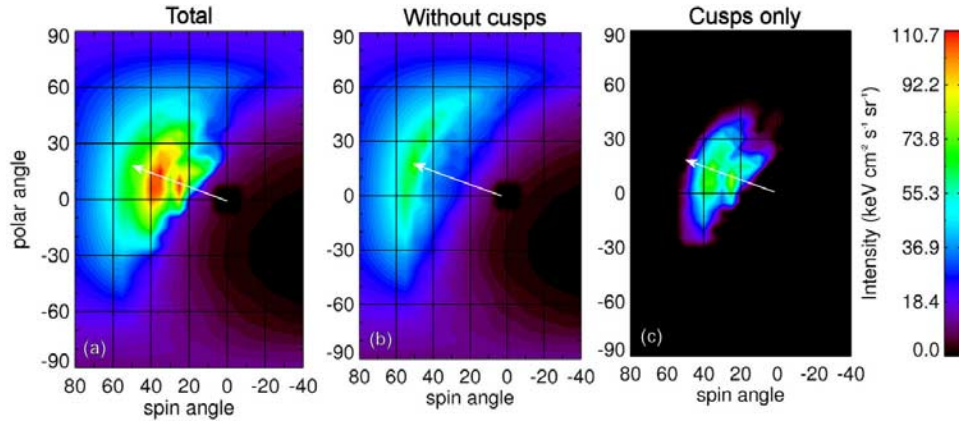


**Figure 2.** (a) Sky map of SWCX X-ray intensities as observed by a hypothetical X-ray detector on IMAGE. The X-ray emissions from the cusps are dominant. (b) Similar image to Figure 2a, but the contribution from the cusps is omitted. The highest X-ray intensities are now from the subsolar region. (c) Sky map of SWCX X-ray intensities that are generated in the cusps region only. In all cases the perspective is from IMAGE as shown in Figure 1. The arrow indicates the Earth-Sun line. To convert this map to 30.4 nm emission (photons/cm<sup>2</sup>/s/sr), multiply the X-ray intensities by 2.5 (see text for details).

able, albeit with different intensities. The center of the subsolar region is at  $\approx 60^\circ$  spin angle.

### 3. Results

#### 3.1. Simulated Observations From Inside the Magnetosheath

[18] The Imager for Magnetopause to Aurora Global Exploration (IMAGE) spacecraft was launched on 25 March 2000. Its mission is to study the global responses of Earth's magnetosphere and ionosphere to the solar wind [Burch, 2003]. The IMAGE instruments perform neutral atom, ultraviolet, and radio plasma imaging. The Low Energy Neutral Atom (LENA) instrument, although designed to image ionospheric outflow [Moore *et al.*, 2000], can also detect low-energy neutral atoms in the solar wind. These neutral atoms are created when solar wind protons charge exchange with exospheric hydrogen, in particular in the magnetosheath and cusps [e.g., Fok *et al.*, 2004]. IMAGE does not have an instrument on board that can detect X rays. However, in this paper we show what a postulated X-ray instrument on board IMAGE would have observed and how these data would complement the low energy neutral atom data. We do this in the hope that some future mission might include this X-ray capability (see Robertson and Cravens [2003] discussion). Similar to the hypothetical X-ray detector, the majority of the observed LENA magnetosheath emission comes from the subsolar region of the magnetosheath and from the cusps [e.g., Taguchi *et al.*, 2005]. However, X rays are emitted isotropically from any given region, unlike the energetic neutral atoms which are created with preferential directions, and so the two techniques complement each other.

[19] LENA saw some dramatic flux enhancements at 0440 UT on 31 March 2001. At this time the IMF was southward oriented, which allows more solar wind protons to enter the magnetosphere through the cusps. For the same conditions we created an all-sky map of X-ray intensities as observed by our hypothetical detector.

[20] In our model the IMAGE spacecraft was put at the actual location for that date and time, which was [1.972, -0.14, 7.8] in SM coordinates. IMAGE is a spinning spacecraft, and its spin axis is approximately perpendicular to the orbit plane. The spin angle is zero when pointing to Earth. The X-ray intensities observed at that location were calculated for 5 degrees increment view angles in both latitude (polar axis) and longitude (spin axis).

[21] On 31 March 2001 at 0440 UT the spacecraft was located high above the North Pole (see Figure 1). Figure 2a shows the sky map generated by our model and as seen by our hypothetical X-ray detector on IMAGE. The point [0,0] is the look direction from IMAGE to Earth. The dark region of the image is the magnetotail region and the bright region is the subsolar region and the cusps. The resolution is  $73 \times 37$  pixels or  $5^\circ \times 5^\circ$ . For comparison Figure 2b also shows the same sky map but with the cusps left out. If we look at the bright region of Figure 2b around a spin angle of  $60^\circ$ , we can clearly see the subsolar region where the highest intensities are expected if no cusps are present. At a spin angle of 20 degrees where the look direction intersects the lower cusp, we see a larger intensity in Figure 2a than in the subsolar region. A similar enhanced intensity can be seen at 40 degrees spin angle where the look direction intersects the upper cusp. The reason for the higher intensities is the high solar wind density and the much higher neutral hydrogen densities in the cusps, which give rise to higher production rates in the cusp regions. Not all the X-ray intensity that we see in the  $20^\circ$  and  $40^\circ$  look directions is due to just the cusps, and to illustrate this in Figure 2 we also show the difference in intensities by subtracting the intensity map without the cusps from the intensity map with the cusps. The maximum cusps contribution is about  $80.8 \text{ keV cm}^{-2} \text{ s}^{-1} \text{ sr}^{-1}$ , while the total contribution is about  $111 \text{ keV cm}^{-2} \text{ s}^{-1} \text{ sr}^{-1}$ , which means that about 2/3 of the maximum intensity comes from the line of sight intersecting a cusp. The next highest intensity is for the line of sight intersecting

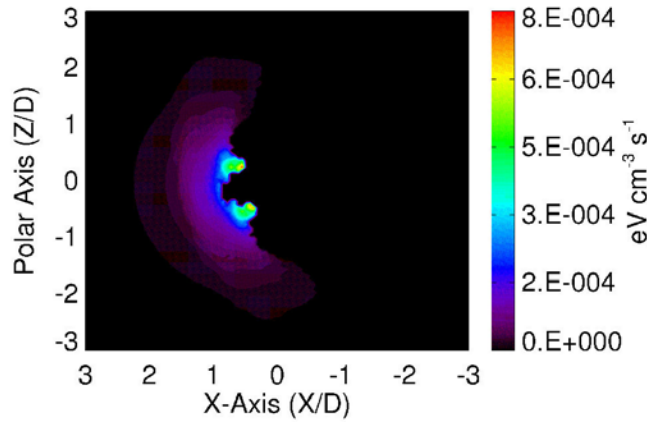


**Figure 3.** X-ray production plot in the GSM  $x$ - $z$  plane. Earth is at  $(0,0)$ . Axes are in distance to the subsolar magnetopause ( $D$ ).

the subsolar region. Clearly, a suitably instrumented spacecraft should be able to detect the cusps in soft X rays.

**3.2. X-Ray Observations From Outside the Magnetosheath**

[22] *Robertson and Cravens* [2003] created images of SWCX X-ray emission as would be seen from an observation point  $50 R_E$  removed from Earth. The observation point was along the  $y$  axis perpendicular to the  $x$ - $z$  plane, where the  $x$  axis is directed from the Earth to the Sun. Average solar wind conditions were used. The cusps were not included in this earlier study. We have now created a similar image, but for the 31 March 2001 event and including the cusps. Figure 3 shows predicted X-ray production rates in the GSM  $x$ - $z$  plane ( $y = 0$ ). Earth is located at the center of the image. The axes are in units of  $D$ , which is the subsolar distance to the magnetopause ( $6 R_E$  in our case). The resolution is  $101 \times 101$  pixels, which is sufficiently high for the cusps to be evident.

[23] The cusps do not extend all the way to Earth because in our current simulations it is impossible to identify purely

solar wind plasma close to Earth. Similar to modeled observations made by a hypothetical X-ray detector on IMAGE, the production rate is clearly at a maximum in the cusp region, with a secondary maximum in the subsolar region. In the flanks and tail region, where the solar wind density is much lower, the production rates are significantly lower too.

[24] Integration along each of the  $101 \times 101$  lines of sight produces the image of SWCX soft X-ray emission (see Figure 4, left side). The largest X-ray intensities are for the cusps, followed by a secondary maximum in the subsolar region (40% less than in the cusps). Because the lines of sight intersect the flanks, the bowshock and the magnetopause are more diffuse, but can still be seen clearly. The maximum subsolar X-ray intensity is twice the intensity that would be seen from inside the magnetosheath due to the geometrical effects.

[25] *Robertson and Cravens* [2003] showed images from “the outside” for a subsolar magnetopause distance of  $9.5 R_E$  (see right side of Figure 4). The upstream solar wind density for that paper was  $7 \text{ cm}^{-3}$  and the speed was 400 km/s. The maximum intensity obtained for those conditions was about  $8 \text{ keV cm}^{-2} \text{ s}^{-1} \text{ sr}^{-1}$ , which was in the subsolar region. On the other hand the maximum predicted intensity for the subsolar region for the 31 March 2001 conditions is about  $160 \text{ keV cm}^{-2} \text{ s}^{-1} \text{ sr}^{-1}$ , which is a factor of 20 greater than the maximum values *Robertson and Cravens* [2003] obtained for average solar wind conditions. This clearly shows the time variability of X-ray emissions produced by the SWCX mechanism as well as the highly nonlinear response of the intensity as the magnetopause moves closer to the Earth. This behavior is similar to that actually observed in the low-energy neutral atom data and simulations.

[26] Charge transfer between solar wind alpha particles and neutral hydrogen produces  $\text{He}^+ 30.4 \text{ nm}$  emission [*Gruntman*, 2001]. This process is essentially the same as the soft X-ray process except that the  $\text{He}^{++}$  charge exchange cross sections are more velocity dependent and somewhat smaller than the heavier ion cross sections. The intensity maps in Figures 2 and 4 can easily be converted to

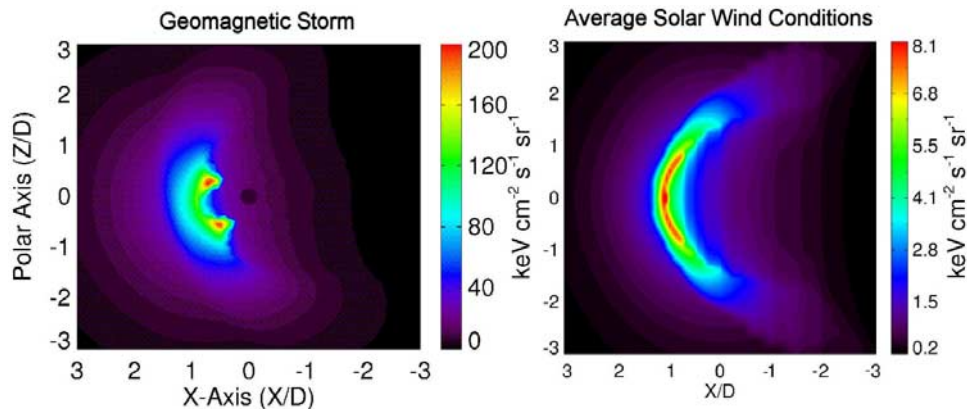


**Figure 4.** X-ray intensities for the 31 March 2001 event, as observed from the GSM  $y$  axis  $50 R_E$  removed from Earth (left). Units are in  $D$ , distance to the subsolar magnetopause. The right side was modeled by *Robertson and Cravens* [2003] for average solar wind conditions. Note that the color scales of the two panels differ. To convert this map to  $30.4 \text{ nm}$  emission ( $\text{photons/cm}^2/\text{s}/\text{sr}$ ), multiply the X-ray intensities by 2.5 (see text for details).

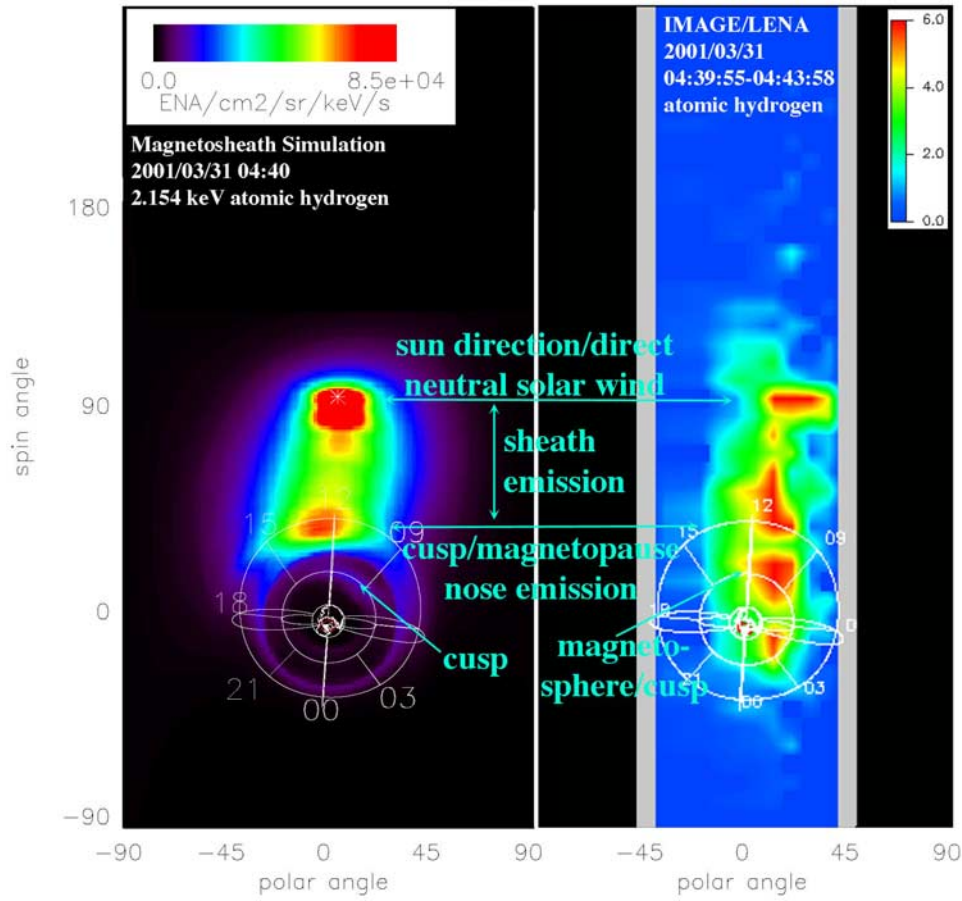


**Figure 5.** Energetic neutral atom data and simulation for 31 March 2001 at 0440 UT. The right panel shows observations from LENA while the left panel is a simulated image. The labels interpret features in the simulation and data based on Figure 1. In these images, the red region in the sun direction is neutral solar wind formed outside the bow shock which does not show up in the X-ray sky maps (see text). The unit conversion is discussed in the text.

approximately 30.4 nm intensity maps. The reason that these maps are “approximately” 30.4 nm is that the 30.4 nm cross sections depend on solar wind speed. If we substitute an estimated efficiency factor  $\alpha_{\text{He}^{++}}$  of  $1.3 \times 10^{-18} \text{ cm}^2$  (see *Robertson and Cravens* [2003] for more details) into equation (2) and integrate this result over a line of sight, we relate the 30.4 nm intensity to the soft X-ray intensity with the expression  $4\pi I_{\text{He}^{++}} \approx 2.5 \times 4\pi I_{\text{X-ray}}$ , where  $I_{\text{X-ray}}$  has units of  $\text{keV cm}^{-2} \text{ s}^{-1}$ . Consequently the maps of Figures 2 and 4 can be converted to 30.4 nm emission maps (with units of  $\text{photons cm}^{-2} \text{ s}^{-1} \text{ sr}^{-1}$ ) by multiplying the X-ray intensities by a factor of 2.5.

[27] *Robertson and Cravens* [2003] calculated that for average solar wind conditions it would be possible to detect SWCX X-ray emissions. They placed a hypothetical X-ray telescope at a distance of  $\sim 20 R_E$  and estimated that with about 100 pixels with a pixel size of  $3^\circ \times 3^\circ$  and for an exposure time of  $\sim 2$  hours, the effective detector area would need to be  $\sim 10 \text{ cm}^2$ , which is considerably smaller than the  $50 \text{ cm}^2$  effective area for the Röntgen satellite’s PSPC instrument 1/4 keV channel. In order to image the bowshock and the magnetosheath, the ideal location of the telescope would be in the flank region outside the magnetosheath.

[28] To summarize this section of the paper, *Robertson and Cravens* [2003] postulated that it was possible to image the magnetosheath in X-rays. They suggested that there was enough time variation in the geocoronal X-ray emission to be able to subtract the steady state X-ray background from the highly variable geocoronal X-ray emission. By studying this new case of X-ray emission for an extremely active event, we can see the possible upper limit of such a time variation, which is significantly different from average solar wind conditions. This affirms the idea that it should be possible to image the magnetosheath from the outside in X rays.

### 3.3. Low-Energy Neutral Atoms

[29] The solar wind also contains earthward directed neutral atoms which are formed through interaction between the solar wind and interstellar neutrals, exospheric neutrals, and dust [*Moore et al.*, 2003]. The LENA instrument on the IMAGE spacecraft, which responds to neutral atoms with energies as low as about 10 eV to energies greater than a few keV, has detected these neutral solar wind atoms [*Collier et al.*, 2001]. During periods of high solar wind flux, the neutral solar wind fluxes are also elevated, frequently by factors much greater than the ionized solar wind

[Collier *et al.*, 2005]. Neutral solar wind correlates well with ionized solar wind and exhibits many similar properties [Pilkerton *et al.*, 2005]. Neutral solar wind has also been observed by Mars Express/ASPERA-3 as the spacecraft was moving into eclipse [Brinkfeldt, 2005].

[30] During the 31 March 2001 event, because of the very high solar wind flux, the LENA instrument observed a much higher than normal emission in the magnetosheath direction. Figure 5 shows the neutrals as observed by LENA (right) and as simulated by the CCMC (left) [Fok *et al.*, 2004] at the time of the simulation in Figure 1, 0440 UT. If we use  $8.5 \times 10^4/\text{cm}^2/\text{sr}/\text{keV}/\text{s}$  for the peak flux, we get  $8.5 \times 10^4/\text{cm}^2/\text{sr}/\text{keV}/\text{s} \times 2 \text{ keV (passband)} \times 0.02 \text{ sr (pixel size)} = 3400/\text{cm}^2/\text{s}$ . For the observations, we get six counts in two spins, which is  $6 \text{ cts}/2 \text{ (spins)}/2.67 \text{ (time/spin)}/1 \text{ cm}^2 \text{ (aperture)}/2 \text{ (energy dep. of eff.)}/1.9 \times 10^{-4} \text{ (1 keV eff.)} = 2960/\text{cm}^2/\text{s}$ . Consequently, the maximum fluxes seen in an  $8^\circ \times 8^\circ$  (0.02 sr) pixel will be about  $3000/\text{cm}^2/\text{s}$  and the simulation and observations agree roughly.

[31] In both panels of Figure 5, the  $y$  axis shows the spin angle with zero degrees pointing toward Earth (nadir). The features in both panels of Figure 5 have been labeled in a way that is guided by the simulation shown in Figure 1. There is some distortion in the polar angle response of the LENA data due to scattering from the conversion surface used to convert incident neutral atoms into negative ions and due to some degradation in the position sensing subsystem which occurred late in year 2000.

[32] The red regions in the left and right panels at spin angles slightly above 90 degrees show the neutral solar wind which has charge exchanged prior to the shock and is hence directional, like the ionized solar wind [Pilkerton *et al.*, 2005]. The broad diffuse emission observed between 90 degrees and 45 degrees seen in both the simulation and data is characteristic of hot, postshock solar wind in the magnetosheath charge-exchanging with exospheric hydrogen. The red region close to 40 degrees is reasonably identified as emission from the cusp and magnetopause nose, as illustrated in Figure 1. Note that the neutral atom emission maximum near the cusp occurs at about the same location in the sky as the X-ray maximum (see Figure 2), as it should. Because the simulation focused on the solar wind and magnetosheath/exosphere interaction, charge exchange close to the Earth was not considered. Consequently, the two large emission regions on the limb of the Earth in the LENA data on the right do not appear in the simulated image on the left. However, there is a faint hint of an enhancement in the simulation which may reasonably be identified on the basis of Figure 1 with the other cusp region. In the LENA image, the cusp signal is likely masked by more intense signals of magnetospheric origin.

[33] In summary, the observations during this period appear to agree well with the neutral atom fluxes inferred from the BATSRUS MHD model. See Moore *et al.* [2003] for more discussion of the LENA observations on this day and their relationship to cusp structure.

[34] Although IMAGE does not carry an X-ray instrument, the results of this study and previous work show that because the underlying physical processes are essentially the same, namely solar wind charge exchange with exo-

spheric neutral hydrogen, X-ray imaging of the magnetosheath would produce images similar to those obtained in low energy neutral atoms.

[35] However, there are notable differences between the two techniques. First, solar wind neutral atoms are primarily hydrogen resulting from protons, whereas X-ray emissions are photons resulting from charge exchange with high charge state heavy ions.

[36] Thus X-ray emission may allow inference of solar wind composition, whereas neutral atom imaging will not [Schwadron and Cravens, 2000]. Second, energetic hydrogen atoms formed by solar wind charge exchange will move in largely the same direction as the initial proton so that neutral atom imaging will provide information on flow direction, but only if the observations are made into the flow direction. X rays, on the other hand, are emitted isotropically so that there is no requirement that the observations be made into the flow direction, but the observations do not contain information on the flow pattern. Third, neutral hydrogen moves effectively at the speed of the proton prior to charge exchange. This produces delays and velocity dispersion that could be used to infer characteristics such as source distance. X rays, of course, move at the speed of light so that the time of observation, at least within the geocoronal context, is essentially the time at which the charge exchange occurred. These differences mean that low-energy neutral atom imaging and X-ray imaging would serve as highly complementary techniques for determining global magnetosheath and cusp properties.

#### 4. Conclusions

[37] The study of the 31 March 2001 event shows us that there are dramatic time variations in X-ray intensities associated with X rays produced by the SWCX mechanism near the Earth. Note that this time variability will facilitate the removal of the steady state X-ray emissions (associated with the heliosphere and “cosmic” sources such as the interstellar medium) and allow the magnetosheath contribution to be seen.

[38] We have demonstrated that particularly high X-ray emissions should originate in the cusps. Previously, Robertson and Cravens [2003] showed that it is possible to remotely observe the magnetosheath from outside the bow shock. The current study shows that the cusps should be observable both from inside the magnetosphere and from outside the bow shock. SWCX X-ray observations are similar to modeled LENA observations; both show the time variability of the solar wind.

[39] **Acknowledgments.** The work at the University of Kansas was supported by the National Science Foundation under grant ATM-0234271. Thanks also to the CCMC and the IMAGE Mission at GSFC for support.

[40] Zuyin Pu thanks Vasili Kharchenko and Thomas Moore for their assistance in evaluating this paper.

#### References

- Baker, D. N., R. E. Ergun, J. L. Burch, J.-M. Jahn, P. W. Daly, R. Friedel, G. D. Reeves, T. A. Fritz, and D. G. Mitchell (2002), A telescopic and microscopic view of a magnetospheric substorm on 31 March 2001, *Geophys. Res. Lett.*, 29(18), 1862, doi:10.1029/2001GL014491.

- Bhardwaj, A., et al. (2002), Soft X-ray emissions from planets, moons, and comets, in *Earth-Like Planets and Moons, Proceedings of the 36th ESLAB Symposium*, edited by B. Foing and B. Battrock, *Eur. Space Agency Spec. Publ., ESA SP-514*, 215–226.
- Bochsler, P., J. Geiss, and R. Joos (1985), Kinetic temperatures of heavy ions in the solar wind, *J. Geophys. Res.*, *90*, 10,779.
- Brinkfeldt, K. (2005), Instrumentation for energetic neutral atom measurements at Mars, Venus, and the Earth, *IRF Sci. Rep. 288*, Swedish Inst. of Space Phys., Kiruna.
- Burch, J. L. (2003), The first two years of IMAGE, *Space Sci. Rev.*, *109*, 1.
- Chapman, S., and V. C. A. Ferraro (1931), A new theory of magnetic storms: 1. The initial phase, *J. Geophys. Res.*, *36*, 171.
- Collier, M. R., D. C. Hamilton, G. Gloeckler, P. Bochsler, and R. B. Sheldon (1996), Neon-20, Oxygen-16, and Helium-4 densities, temperatures, and suprathermal tails in the solar wind determined with WIND/MASS, *Geophys. Res. Lett.*, *23*, 1191.
- Collier, M. R., et al. (2001), Observations of neutral atoms from the solar wind, *J. Geophys. Res.*, *106*, 24,893.
- Collier, M. R., T. E. Moore, M.-C. Fok, B. Pilkerton, and S. Boardsen (2005), Low-energy neutral atom signatures of magnetopause motion in response to southward Bz, *J. Geophys. Res.*, *110*, A02102, doi:10.1029/2004JA010626.
- Cravens, T. E. (1997), Comet Hyakutake X-ray source: Charge transfer of solar wind heavy ions, *Geophys. Res. Lett.*, *24*, 105.
- Cravens, T. E. (2000), Heliospheric X-ray emission associated with charge transfer of the solar wind with interstellar neutrals, *Astrophys. J.*, *532*, L153.
- Cravens, T. E. (2002), X-ray emission from comets, *Science*, *296*, 1042.
- Cravens, T. E., I. P. Robertson, and S. L. Snowden (2001), Temporal variations of geocoronal and heliospheric X-ray emission associated with the solar wind interaction with neutrals, *J. Geophys. Res.*, *106*, 24,883.
- Feynman, J. (1975), On solar wind helium and heavy ion temperatures, *Solar Phys.*, *43*, 249.
- Fok, M.-C., T. E. Moore, and M. R. Collier (2004), Neutral atom imaging of solar wind interaction with Earth and Venus, *J. Geophys. Res.*, *109*, A01206, doi:10.1029/2003JA010094.
- Groth, C. P. T., D. L. Zeeuw, T. I. Gombosi, and K. G. Powell (2000), Global three-dimensional MHD simulation of a space weather event: CME formation, interplanetary propagation, and interaction with the magnetosphere, *J. Geophys. Res.*, *105*, 25,053.
- Gruntman, M. (2001), Imaging the three-dimensional solar wind, *J. Geophys. Res.*, *106*, 8205.
- Hodges, R. R., Jr. (1994), Monte Carlo simulation of the terrestrial hydrogen exosphere, *J. Geophys. Res.*, *99*, 23,229.
- Kharchenko, V., and A. Dalgarno (2000), Spectra of cometary X-rays induced by solar wind minor ions, *J. Geophys. Res.*, *105*, 18,351.
- Krasnopolsky, V. A., J. B. Greenwood, and P. C. Stancil (2005), X-ray and extreme ultraviolet emissions from comets, *Space Sci. Rev.*, *113*, 271.
- Lisse, C. M., et al. (1996), Discovery of X-ray and extreme ultraviolet emission from Comet C/Hyakutake 1996 B2, *Science*, *274*, 205.
- Lisse, C. M., K. Dennerl, J. Englhauser, J. Trümper, F. E. Marshall, R. Petre, A. Valine, B. J. Kellett, and R. Bingham (1999), X-ray emission from comet Hale-Bopp, *Earth Moon Planets*, *77*, 283.
- Lisse, C. M., et al. (2005), Chandra observations of comet 2P/Encke 2003: First detection of a collisionally thin, fast solar wind charge exchange system, *Astrophys. J.*, *635*, 1329.
- Moore, T. E., et al. (2000), The Low-Energy Neutral Atom Imager for IMAGE, *Space Sci. Rev.*, *109*, 155.
- Moore, T. E., M. R. Collier, M.-C. Fok, S. A. Fuselier, S. H. Khan, W. Lennartsson, D. G. Simpson, G. R. Wilson, and M. O. Chandler (2003), Heliosphere-geosphere interactions using low-energy neutral atom energy, *Space Sci. Rev.*, *109*, 351.
- Neugebauer, M., T. E. Cravens, C. M. Lisse, F. M. Ipavich, R. von Steiger, P. D. Shah, and T. P. Armstrong (2000), Time variabilities of soft X-ray emission from comet Hyakutake and solar wind ion fluxes, *J. Geophys. Res.*, *105*, 20,949.
- Ogilvie, K. W., P. Bochsler, J. Geiss, and M. A. Coplan (1980), Observations of the velocity distribution of solar wind ions, *J. Geophys. Res.*, *85*, 6069.
- Pepino, R., V. Kharchenko, A. Dalgarno, and R. Lallement (2004), Spectra of the X-ray emission induced in the interaction between the solar wind and heliospheric gas, *Astrophys. J.*, *617*, 1347.
- Pilkerton, B. M., M. R. Collier, and T. E. Moore (2005), Correlations between neutral and ionized solar wind, *Adv. Space Res.*, *35*, 2152.
- Reiff, P. H., T. W. Hill, and J. L. Burch (1977), Solar wind plasma injections at the dayside magnetospheric cusp, *J. Geophys. Res.*, *82*, 479.
- Robertson, I. P., and T. E. Cravens (2003), X-ray emission from the terrestrial magnetosheath, *Geophys. Res. Lett.*, *30*(8), 1439, doi:10.1029/2002GL016740.
- Schwadron, N. A., and T. E. Cravens (2000), Cometary X-ray emission for slow and fast solar wind, *Astrophys. J.*, *544*, 558.
- Snowden, S. L., M. R. Collier, and K. D. Kuntz (2004), XMM-Newton observation of solar wind charge exchange emission, *Astrophys. J.*, *610*, 1182.
- Spreiter, J. R., A. L. Summers, and A. Y. Alksne (1966), Hydromagnetic flow around the magnetosphere, *Planet. Space Sci.*, *14*, 223.
- Taguchi, S., M. R. Collier, T. E. Moore, M.-C. Fok, and H. J. Singer (2004), Response of neutral atom emissions in the low-latitude and high-latitude magnetosheath direction to the magnetopause motion under extreme solar wind conditions, *J. Geophys. Res.*, *109*, A04208, doi:10.1029/2003JA010147.
- Taguchi, S., S.-H. Chen, M. R. Collier, T. E. Moore, M.-C. Fok, K. Hosokawa, and A. Nakao (2005), Monitoring the high-altitude cusp with low-energy neutral atom imager: Simultaneous observations from IMAGE and Polar, *J. Geophys. Res.*, *110*, A12204, doi:10.1029/2005JA011075.
- Wargelin, B. J., M. Markevitch, M. Juda, V. Kharchenko, R. Edgar, and A. Dalgarno (2004), CHANDRA observations of the “dark” moon and geocoronal solar wind charge exchange, *Astrophys. J.*, *607*, 596.

---

M. R. Collier and M.-C. Fok, Heliospheric Physics, NASA Goddard Space Flight Center, Greenbelt, MD 20771, USA.

T. E. Cravens and I. P. Robertson, Department of Physics and Astronomy, University of Kansas, Lawrence, KS, USA. (robertin@ku.edu)